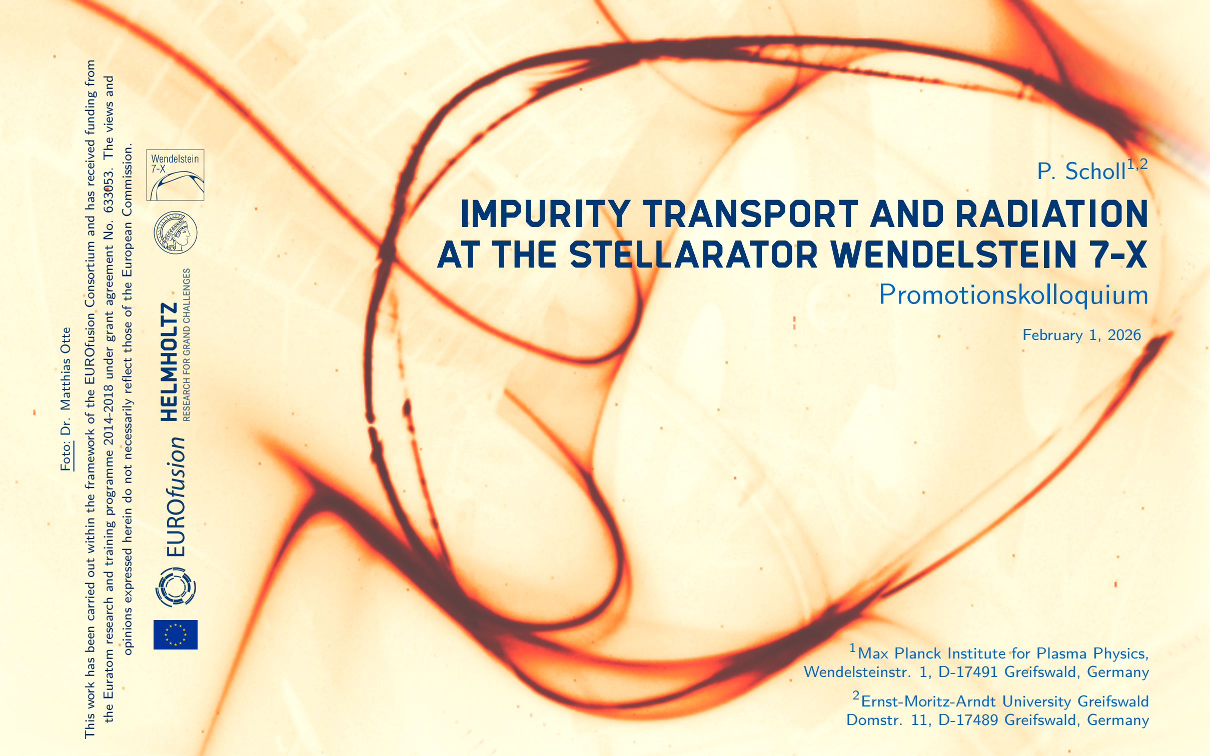

P. Scholl[1,2]

IMPURITY TRANSPORT AND RADIATION AT THE STELLARATOR WENDELSTEIN 7-X

Promotionskolloquium

February 1, 2026

[1]Max Planck Institute for Plasma Physics,
Wendelsteinstr. 1, D-17491 Greifswald, Germany

[2]Ernst-Moritz-Arndt University Greifswald
Domstr. 11, D-17489 Greifswald, Germany

Foto: Dr. Matthias Otte

This work has been carried out within the framework of the EUROfusion Consortium and has received funding from the Euratom research and training programme 2014-2018 under grant agreement No. 633053. The views and opinions expressed herein do not necessarily reflect those of the European Commission.

CONTENTS

MOTIVATION AND CONTEXT

NUCLEAR FUSION: THE ENERGY CHALLENGE

- D-T fusion reaction: ^{2}H + ^{3}H $\rightarrow$ ^{4}He (3.5 MeV) + n (14.1 MeV)
- Lawson criterion for net energy gain:

$$n_e T \tau_E \geq \frac{12 f_{tot}}{\langle \sigma_{DT} v \rangle f_H^2 E_\alpha - 4 L_Z(T)} T^2$$

- Requires: high temperature ($T \sim$ 10-20 keV), density, and confinement time
- Magnetic confinement: tokamaks and stellarators

NUCLEAR FUSION: THE ENERGY CHALLENGE

- D-T fusion reaction: ^{2}H + ^{3}H $\rightarrow$ ^{4}He (3.5 MeV) + n (14.1 MeV)
- Lawson criterion for net energy gain:

$$n_e T \tau_E \geq \frac{12 f_{tot}}{\langle \sigma_{DT} v \rangle f_H^2 E_\alpha - 4 L_Z(T)} T^2$$

- Requires: high temperature ($T \sim$ 10-20 keV), density, and confinement time
- Magnetic confinement: tokamaks and stellarators

Triple Product

Key figure of merit for fusion performance combining density, temperature, and energy confinement time

WENDELSTEIN 7-X STELLARATOR

- World's largest stellarator ($R = 5.5$ m, $a \sim 0.5$ m)
- 50 superconducting coils, 5-fold symmetry
- Island divertor configuration
- Optimized for reduced neoclassical transport
- Operational phases: OP1.1, OP1.2a, OP1.2b
- Achieved 30 minute plasma discharges

Wendelstein 7-X Stellarator

- World's largest stellarator ($R = 5.5$ m, $a \sim 0.5$ m)
- 50 superconducting coils, 5-fold symmetry
- Island divertor configuration
- Optimized for reduced neoclassical transport
- Operational phases: OP1.1, OP1.2a, OP1.2b
- Achieved 30 minute plasma discharges

Key Challenge

Managing heat loads on plasma-facing components through controlled radiative cooling

PLASMA RADIATION AND TRANSPORT

Transport Mechanisms:

- Classical: collisional diffusion
- Neoclassical: trapped particles, $\propto 1/\nu$
- Anomalous: turbulent transport (dominant)

Radiation Processes:

- Bremsstrahlung: $P_{Brems} \propto n_e^2 T^{1/2}$
- Line radiation: atomic transitions
- Impurity effects on plasma performance

PLASMA RADIATION AND TRANSPORT

Transport Mechanisms:

- Classical: collisional diffusion
- Neoclassical: trapped particles, $\propto 1/\nu$
- Anomalous: turbulent transport (dominant)

Radiation Processes:

- Bremsstrahlung: $P_{Brems} \propto n_e^2 T^{1/2}$
- Line radiation: atomic transitions
- Impurity effects on plasma performance

PLASMA RADIATION AND TRANSPORT

Transport Mechanisms:

- Classical: collisional diffusion
- Neoclassical: trapped particles, $\propto 1/\nu$
- Anomalous: turbulent transport (dominant)

Radiation Processes:

- Bremsstrahlung: $P_{Brems} \propto n_e^2 T^{1/2}$
- Line radiation: atomic transitions
- Impurity effects on plasma performance

Impurity Seeding

Deliberate injection of low-Z (He, N_2) or high-Z (Ne, Ar) impurities to enhance edge cooling and achieve detachment

Radiation Fraction:

$$f_{rad} = \frac{P_{rad}}{P_{ECRH}}$$

BOLOMETER DIAGNOSTIC SYSTEM

BOLOMETRY AT W7-X

Metal Resistor Bolometers:

- Thin metal film absorbers (Pt, Au)
- Wheatstone bridge circuit
- Measures total radiation power
- Multicamera system: HBC, VBCl, VBCr
- 128 channels total
- Spatial resolution: ∼5 cm at magnetic axis

BOLOMETRY AT W7-X

Metal Resistor Bolometers:

- Thin metal film absorbers (Pt, Au)
- Wheatstone bridge circuit
- Measures total radiation power
- Multicamera system: HBC, VBCl, VBCr
- 128 channels total
- Spatial resolution: ~5 cm at magnetic axis

Measurement Principle:

$$P_M = F_M \cdot \left(\frac{d(\Delta \widetilde{U}_M)}{dt} + f_M \Delta \widetilde{U}_M \right)$$

Global Radiation Power:

$$P_{rad} = \frac{V_{P,tor}}{V_C} \sum_M \frac{P_M V_M}{K_M}$$

BOLOMETER CALIBRATION AND PERFORMANCE

Calibration Methods:

- In-situ laser calibration
- Electrical calibration
- Etendue calculations:
  $K_M = \int_M \widetilde{K}_M dA_M$
- Volume determination: V_M (LOS cone volume)

Performance Characteristics:

- Time resolution: $\sim$1 ms
- Sensitivity: $\sim$10 kW/m^3
- Uncertainty: $\sim$10-15%

BOLOMETER CALIBRATION AND PERFORMANCE

Calibration Methods:

- In-situ laser calibration
- Electrical calibration
- Etendue calculations:
  $K_M = \int_M \widetilde{K}_M dA_M$
- Volume determination: V_M (LOS cone volume)

Performance Characteristics:

- Time resolution: $\sim$1 ms
- Sensitivity: $\sim$10 kW/m^3
- Uncertainty: $\sim$10-15%

BOLOMETER CALIBRATION AND PERFORMANCE

Calibration Methods:

- In-situ laser calibration
- Electrical calibration
- Etendue calculations: $K_M = \int_M \widetilde{K}_M dA_M$
- Volume determination: V_M (LOS cone volume)

Performance Characteristics:

- Time resolution: $\sim$1 ms
- Sensitivity: $\sim$10 kW/m^3
- Uncertainty: $\sim$10-15%

Chord Brightness

Line-integrated measurement along each detector's line of sight provides radial profile information

Applications:

- Power balance calculations
- Radiation profile monitoring
- Real-time feedback control
- Tomographic reconstruction

REAL-TIME RADIATION FEED-BACK CONTROL

FEEDBACK SYSTEM DESIGN

System Architecture:

- NI 6321 data acquisition hardware
- LabVIEW control software
- PID controller implementation
- Thermal gas valve actuation
- Minimum latency: 13.6 ms

PID Controller:

$$u(t) = K_p e(t) + K_i \int e(t')dt' + K_d \frac{de(t)}{dt}$$

FEEDBACK SYSTEM DESIGN

System Architecture:

- NI 6321 data acquisition hardware
- LabVIEW control software
- PID controller implementation
- Thermal gas valve actuation
- Minimum latency: 13.6 ms

PID Controller:

$$u(t) = K_p e(t) + K_i \int e(t')dt' + K_d \frac{de(t)}{dt}$$

Radiation Prediction Proxies:

Subset-based (3-7 channels):

$$P^{(1)}_{pred} = \frac{V_{P,tor}}{V_S} \sum_{M}^{S} \frac{P_M V_M}{K_M}$$

Single channel (dimensionless):

$$P^{(2)}_{pred} \propto \Delta U_M$$

EXPERIMENTAL ACHIEVEMENTS

XP20181010.32 - Benchmark Discharge:

- Stable helium-seeded detachment
- Radiation fraction: $f_{rad} > 90\%$
- Peak values up to 100%
- Target heat load reduction: factor of 2
- C^{3+} detachment at $f_{rad} \sim 50\%$
- Validated 3-channel LOS subset

EXPERIMENTAL ACHIEVEMENTS

XP20181010.32 - Benchmark Discharge:

- Stable helium-seeded detachment
- Radiation fraction: $f_{rad} > 90\%$
- Peak values up to 100%
- Target heat load reduction: factor of 2
- C^{3+} detachment at $f_{rad} \sim 50\%$
- Validated 3-channel LOS subset

Key Result

Demonstrated stable, feedback-controlled radiative cooling with $f_{rad} \geq 85\%$ without terminal plasma disruption

Comparison with Other Methods:

- Electron density feedback
- C-III filterscope feedback
- Bolometer feedback shows intrinsic connection to detachment physics

FEEDBACK PERFORMANCE ANALYSIS

- **Gas Injection Dynamics:** Moderately scaled gas puffs (medium length and intensity) most effective for reliable edge cooling
- **System Limitations:** Computational and algorithmic constraints introduce non-negligible latencies
- **Optimization Challenges:** Difficult to optimize during commissioning due to limited experimental time

FEEDBACK PERFORMANCE ANALYSIS

- **Gas Injection Dynamics:** Moderately scaled gas puffs (medium length and intensity) most effective for reliable edge cooling
- **System Limitations:** Computational and algorithmic constraints introduce non-negligible latencies
- **Optimization Challenges:** Difficult to optimize during commissioning due to limited experimental time

Critical Finding

The intrinsic connection of P_{rad} and f_{rad} to the detachment process makes bolometer feedback essential for future fusion reactor applications

LINE OF SIGHT SENSITIVITY AND MODELING

IMPURITY SEEDING MODELS

Two-Chamber Model:

$$\dot{N}_\mathrm{w} = \left(N_\mathrm{w,lim} - N_\mathrm{w}\right) \tau_\mathrm{w,p}$$
$$\dot{N}_\mathrm{p} = \Gamma_\mathrm{s} + N_\mathrm{w}\tau_\mathrm{w,p} - f_\mathrm{w,p}N_\mathrm{p} - N_\mathrm{p}\tau_\mathrm{p}$$

- Plasma and wall compartments
- Particle exchange rates
- Pumping and recycling

IMPURITY SEEDING MODELS

Two-Chamber Model:

$$\dot{N}_\mathrm{w} = \left(N_\mathrm{w,lim} - N_\mathrm{w}\right)\tau_\mathrm{w,p}$$
$$\dot{N}_\mathrm{p} = \Gamma_\mathrm{s} + N_\mathrm{w}\tau_\mathrm{w,p} - f_\mathrm{w,p}N_\mathrm{p} - N_\mathrm{p}\tau_\mathrm{p}$$

- Plasma and wall compartments
- Particle exchange rates
- Pumping and recycling

Three-Chamber Model:

$$\dot{N}_\mathrm{w} = \left(N_\mathrm{w,lim} - N_\mathrm{w}\right)\tau_\mathrm{w,s}$$
$$\dot{N}_\mathrm{s} = \Gamma_\mathrm{s} - N_\mathrm{s}\left(\tau_\mathrm{s,p} + \tau_\mathrm{s}\right) + g\left(N_\mathrm{P}, N_\mathrm{S}\right) - c_0$$
$$\dot{N}_\mathrm{p} = N_\mathrm{s}\tau_\mathrm{s,p} - \frac{N_\mathrm{p}N_\mathrm{s}}{N_\mathrm{p,lim}}$$

- Adds SOL compartment
- Better represents edge physics
- Both models equally capable of representing feedback measurements

CHANNEL SELECTION SENSITIVITY

LOS Sensitivity Evaluation:

- Weighted deviation metric
- Correlation analysis
- Mean deviation assessment

Optimal Channel Selection:

- No single "best" set exists
- Robust selection achieves $\geq$85% prediction accuracy
- Agreement between HBC and VBC cameras

CHANNEL SELECTION SENSITIVITY

LOS Sensitivity Evaluation:

- Weighted deviation metric
- Correlation analysis
- Mean deviation assessment

Optimal Channel Selection:

- No single "best" set exists
- Robust selection achieves $\geq$85% prediction accuracy
- Agreement between HBC and VBC cameras

Key Finding

Detectors viewing separatrix and SOL region most viable for real-time feedback configurations

STRAHL IMPURITY TRANSPORT MODELING

STRAHL Code:

- 1D impurity transport simulation
- Models carbon and oxygen radiation
- Includes ionization, recombination
- Diffusion and convection transport

Key Results:

- Carbon dominates SOL emissivity
- Reduced diffusivity near separatrix
- Inward shift of radiation for $f_{rad} \to 1$
- Radiation moves from outside to inside separatrix

STRAHL IMPURITY TRANSPORT MODELING

STRAHL Code:

- 1D impurity transport simulation
- Models carbon and oxygen radiation
- Includes ionization, recombination
- Diffusion and convection transport

Forward Modeling:

- Calculate chord brightness from STRAHL profiles
- Compare with experimental measurements
- Validate transport assumptions

Key Results:

- Carbon dominates SOL emissivity
- Reduced diffusivity near separatrix
- Inward shift of radiation for $f_{rad} \to 1$
- Radiation moves from outside to inside separatrix

Discrepancy

Forward calculations show less asymmetry in chord brightness than experiments, suggesting model limitations in capturing 3D effects

TOMOGRAPHIC RECONSTRUCTION

MINIMUM FISHER REGULARIZATION (MFR)

Ill-Posed Inverse Problem:

- 128 line-integrated measurements
- Reconstruct 2D emissivity: ∼4500 pixels
- Requires regularization

Fisher Information:

$$I_F = \int \frac{1}{g(\vec{r})} \left(\frac{\partial g(\vec{r})}{\partial \vec{r}} \right)^2 d\vec{r}$$

Iterative Solution:

$$\vec{x}^{(n+1)} = \left(\mathbf{T}^T \mathbf{T} + \mu \mathbf{H}^{(n)} \right)^{-1} \mathbf{T}^T \vec{b}$$

Radially Dependent Anisotropy (RDA):

- Tailored weighting: $k_{ani}(r)$
- $k < 1$: localized structures
- $k > 1$: smooth distributions
- Separate core and edge parameters

MFR Advantages

- Robust to noisy data
- Smooth solutions
- Incorporates a priori knowledge
- Stable convergence

GEOMETRY SENSITIVITY AND BENCHMARKING

Geometry Perturbation Tests:

- Camera position variations
- Detector/aperture segmentation (N=2,4,8)
- Triangulation vs rectangular splitting
- Etendue calculation validation

GEOMETRY SENSITIVITY AND BENCHMARKING

Geometry Perturbation Tests:

- Camera position variations
- Detector/aperture segmentation (N=2,4,8)
- Triangulation vs rectangular splitting
- Etendue calculation validation

Key Findings:

- Significant robustness to geometry variations
- $N \geq 8$ segmentation adequate
- Intrinsic bias toward upper SOL/separatrix
- Camera displacement effects non-negligible

GEOMETRY SENSITIVITY AND BENCHMARKING

Phantom Image Benchmarks:

- Simple and complex test profiles
- Quality metrics: χ^2, ρ_c
- Optimal k_{ani} depends on profile
- No universal "best" parameters

GEOMETRY SENSITIVITY AND BENCHMARKING

Phantom Image Benchmarks:

- Simple and complex test profiles
- Quality metrics: χ^2, ρ_c
- Optimal k_{ani} depends on profile
- No universal "best" parameters

Recommended Settings

$k_{ani} = \{2.0, 0.3\}$ (core, edge)
Grid: 30×150 pixels
Domain: $1.3^2 V_P$

EXPERIMENTAL TOMOGRAPHY RESULTS

Statistical Analysis:

- Forward vs backward P_{rad} correlation
- Core radiation slightly overestimated
- Total power significantly overestimated
- Consistent with phantom benchmarks

EXPERIMENTAL TOMOGRAPHY RESULTS

Statistical Analysis:

- Forward vs backward P_{rad} correlation
- Core radiation slightly overestimated
- Total power significantly overestimated
- Consistent with phantom benchmarks

Power Balance Application:

$$P_{bal} = P_{ECRH} - P_{rad} - P_{div}$$

- P_{2D}^{core} improves balance accuracy
- More stable than P_{rad} alone
- Alternative for quasi-steady-state analysis

TOMOGRAPHY QUALITY ASSESSMENT

- **Reconstruction Accuracy:** P_{rad} consistently underestimates total 2D integrated power by amount equal to SOL radiation
- **Quality Metrics:** χ^2 and correlation coefficient ρ_c not always congruent - optimal tomogram may not have $\chi^2 = 1$
- **Anisotropy Optimization:** Ideal k_{ani} set exists for each profile but dimensionality makes finding it impractical
- **Experimental Validation:** Results agree well with phantom benchmarks, supporting algorithm reliability

TOMOGRAPHY QUALITY ASSESSMENT

- **Reconstruction Accuracy:** P_{rad} consistently underestimates total 2D integrated power by amount equal to SOL radiation
- **Quality Metrics:** χ^2 and correlation coefficient ρ_c not always congruent - optimal tomogram may not have $\chi^2 = 1$
- **Anisotropy Optimization:** Ideal k_{ani} set exists for each profile but dimensionality makes finding it impractical
- **Experimental Validation:** Results agree well with phantom benchmarks, supporting algorithm reliability

Conclusion

MFR with RDA weighting provides robust, reliable 2D radiation reconstructions suitable for physics analysis and power balance calculations, though computational limitations prevent continuous real-time operation

CONCLUSIONS AND OUTLOOK

KEY ACHIEVEMENTS

1. **Real-Time Feedback System:** Successfully implemented, tested and operated first bolometer radiation feedback at W7-X
2. **Line of Sight Optimization:** Systematic sensitivity analysis identified optimal detector configurations
3. **Tomographic Reconstruction:** Developed and benchmarked tailored MFR algorithm with RDA weighting

KEY ACHIEVEMENTS

1. **Real-Time Feedback System:** Successfully implemented, tested and operated first bolometer radiation feedback at W7-X
   - Achieved stable detachment with $f_{rad} \geq 85\%$, peaks up to 100%
   - Reduced target heat loads by factor of 2
   - Validated 3-channel LOS subset for fast prediction
2. **Line of Sight Optimization:** Systematic sensitivity analysis identified optimal detector configurations
3. **Tomographic Reconstruction:** Developed and benchmarked tailored MFR algorithm with RDA weighting

KEY ACHIEVEMENTS

1. **Real-Time Feedback System:** Successfully implemented, tested and operated first bolometer radiation feedback at W7-X
   - Achieved stable detachment with $f_{rad} \geq 85\%$, peaks up to 100%
   - Reduced target heat loads by factor of 2
   - Validated 3-channel LOS subset for fast prediction
2. **Line of Sight Optimization:** Systematic sensitivity analysis identified optimal detector configurations
   - Separatrix and SOL viewing channels most effective
   - Robust selection achieves ≥85% prediction accuracy
   - No single "best" set - multiple viable configurations
3. **Tomographic Reconstruction:** Developed and benchmarked tailored MFR algorithm with RDA weighting

KEY ACHIEVEMENTS

1. **Real-Time Feedback System:** Successfully implemented, tested and operated first bolometer radiation feedback at W7-X
   - Achieved stable detachment with $f_{rad} \geq 85\%$, peaks up to 100%
   - Reduced target heat loads by factor of 2
   - Validated 3-channel LOS subset for fast prediction
2. **Line of Sight Optimization:** Systematic sensitivity analysis identified optimal detector configurations
   - Separatrix and SOL viewing channels most effective
   - Robust selection achieves ≥85% prediction accuracy
   - No single "best" set - multiple viable configurations
3. **Tomographic Reconstruction:** Developed and benchmarked tailored MFR algorithm with RDA weighting
   - Robust to geometry perturbations and noise
   - Successfully applied to experimental data
   - Provides alternative for power balance calculations

SCIENTIFIC INSIGHTS

Detachment Physics:

- C^{3+} detachment visible at $f_{rad} \sim 50\%$
- Stable detachment achievable at $f_{rad} > 90\%$
- Radiation shifts inward as $f_{rad} \to 1$
- X-point and island radiation concentration

SCIENTIFIC INSIGHTS

Detachment Physics:

- C^{3+} detachment visible at $f_{rad} \sim 50\%$
- Stable detachment achievable at $f_{rad} > 90\%$
- Radiation shifts inward as $f_{rad} \to 1$
- X-point and island radiation concentration

Impurity Transport:

- Carbon dominates SOL emissivity
- Reduced diffusivity near separatrix
- Complex 3D effects in stellarator geometry

SCIENTIFIC INSIGHTS

Detachment Physics:

- C^{3+} detachment visible at $f_{rad} \sim 50\%$
- Stable detachment achievable at $f_{rad} > 90\%$
- Radiation shifts inward as $f_{rad} \to 1$
- X-point and island radiation concentration

Impurity Transport:

- Carbon dominates SOL emissivity
- Reduced diffusivity near separatrix
- Complex 3D effects in stellarator geometry

Feedback Control:

- Moderate gas puffs most effective
- No simple scaling law found
- Intrinsic connection to detachment essential
- System latency limits performance

SCIENTIFIC INSIGHTS

Detachment Physics:

- C^{3+} detachment visible at $f_{rad} \sim 50\%$
- Stable detachment achievable at $f_{rad} > 90\%$
- Radiation shifts inward as $f_{rad} \to 1$
- X-point and island radiation concentration

Impurity Transport:

- Carbon dominates SOL emissivity
- Reduced diffusivity near separatrix
- Complex 3D effects in stellarator geometry

Feedback Control:

- Moderate gas puffs most effective
- No simple scaling law found
- Intrinsic connection to detachment essential
- System latency limits performance

Diagnostic Performance:

- Multicamera system provides comprehensive coverage
- Geometry uncertainties affect results
- Tomography reveals SOL radiation underestimation

FUTURE OUTLOOK AND RECOMMENDATIONS

System Upgrades:

- Reduce feedback latency through hardware/software optimization
- Implement more complex P_{pred} models
- Per-experiment configurability
- Develop predictive scaling laws

FUTURE OUTLOOK AND RECOMMENDATIONS

System Upgrades:

- Reduce feedback latency through hardware/software optimization
- Implement more complex P_{pred} models
- Per-experiment configurability
- Develop predictive scaling laws

Modeling Improvements:

- Refine multi-chamber models with experimental data
- Integrate with other SOL models
- Better parametric optimization
- 3D effects in STRAHL modeling

FUTURE OUTLOOK AND RECOMMENDATIONS

System Upgrades:

- Reduce feedback latency through hardware/software optimization
- Implement more complex P_{pred} models
- Per-experiment configurability
- Develop predictive scaling laws

Modeling Improvements:

- Refine multi-chamber models with experimental data
- Integrate with other SOL models
- Better parametric optimization
- 3D effects in STRAHL modeling

Tomography Extensions:

- Larger phantom benchmark set
- Additional virtual camera arrays
- Real-time capable algorithms
- Automated parameter optimization

FUTURE OUTLOOK AND RECOMMENDATIONS

System Upgrades:

- Reduce feedback latency through hardware/software optimization
- Implement more complex P_{pred} models
- Per-experiment configurability
- Develop predictive scaling laws

Modeling Improvements:

- Refine multi-chamber models with experimental data
- Integrate with other SOL models
- Better parametric optimization
- 3D effects in STRAHL modeling

Tomography Extensions:

- Larger phantom benchmark set
- Additional virtual camera arrays
- Real-time capable algorithms
- Automated parameter optimization

Reactor Relevance:

- Essential for DEMO power plant operation
- Reliable radiative cooling at $f_{\text{rad}} \geq 95\%$
- Machine protection and heat load management
- Steady-state operation capability

Broader Impact

Contribution to Fusion Energy Research

This thesis advances the state-of-the-art in plasma diagnostics and control for stellarator fusion devices, providing essential tools and knowledge for achieving reactor-relevant operating scenarios with controlled radiative cooling and stable detachment.

BROADER IMPACT

Contribution to Fusion Energy Research

This thesis advances the state-of-the-art in plasma diagnostics and control for stellarator fusion devices, providing essential tools and knowledge for achieving reactor-relevant operating scenarios with controlled radiative cooling and stable detachment.

Technical Contributions:

- First real-time bolometer feedback at W7-X
- Validated diagnostic optimization methods
- Benchmarked tomography algorithm
- Demonstrated stable high-f_{rad} operation

BROADER IMPACT

Contribution to Fusion Energy Research

This thesis advances the state-of-the-art in plasma diagnostics and control for stellarator fusion devices, providing essential tools and knowledge for achieving reactor-relevant operating scenarios with controlled radiative cooling and stable detachment.

Technical Contributions:

- First real-time bolometer feedback at W7-X
- Validated diagnostic optimization methods
- Benchmarked tomography algorithm
- Demonstrated stable high-f_{rad} operation

Scientific Contributions:

- Detachment physics understanding
- Impurity transport insights
- Radiation distribution characterization
- Power balance methodology

SUMMARY

- Developed and operated first real-time bolometer radiation feedback system at W7-X stellarator
- Achieved stable, controlled detachment with radiation fractions $f_{rad} \geq 85\%$ and peaks up to 100%
- Reduced divertor target heat loads by factor of 2 through controlled impurity seeding
- Validated 3-channel bolometer subset for fast radiation power prediction with ≥85% accuracy
- Systematic line of sight sensitivity analysis identified optimal detector configurations for feedback
- STRAHL modeling revealed carbon dominance in SOL radiation and inward shift at high f_{rad}
- Developed and benchmarked Minimum Fisher Regularization tomography with radially dependent anisotropy
- Demonstrated robust 2D radiation reconstruction from experimental data
- Provided alternative power balance methodology using tomographic integrals
- Established essential approach for future fusion reactor heat load management

COLLABORATIONS

Acknowledgement

This work has been carried out within the framework of the EUROfusion Consortium and has received funding from the Euratom research and training programme 2014-2018 under grant agreement No. 633053. The views and opinions expressed herein do not necessarily reflect those of the European Commission.

Collaborators:

Wendelstein 7-X | IPP | HELMHOLTZ RESEARCH FOR GRAND CHALLENGES | EUROfusion

Thank You

Questions?

REFERENCES I